Complex Dynamics in Coupled Cardiac Pacemaker Cells

Dongming Cai,[1,2] Ying-Cheng Lai,[3] and Raimond L. Winslow[2,3,4]

[1]*The Biomedical Engineering Program, The University of Minnesota, Minneapolis, Minnesota 55455*

[2]*The Army High Performance Computing Research Center, The University of Minnesota, Minneapolis, Minnesota 55455*

[3]*The Department of Biomedical Engineering, The Johns Hopkins University School of Medicine, Baltimore, Maryland 21205*

[4]*The Department of Computer Science, The Johns Hopkins University Whiting School of Engineering, Baltimore, Maryland 21205*

(Received 10 May 1993)

We investigate the dynamics of a model of electrically coupled pacemaking cardiac sino-atrial node cells. Cell models are biophysically detailed, and include voltage-dependent membrane currents, pump-exchanger currents, and time-varying internal ion concentration changes similar to those seen in real sino-atrial node cells. It is found that at low, yet physiologically realistic coupling conductance values, complex dynamics including chaos can arise. Occurrence of these complex dynamics in coupled pacemaker cells may provide an explanation for the origin of certain cardiac arrhythmias.

PACS numbers: 87.10.+e, 05.45.+b

The sino-atrial (SA) node, a thin sheet of tissue located in the right atrium at the base of the superior vena cava, is the natural pacemaker of the heart. When isolated, each node cell undergoes spontaneous oscillation, exhibiting a distinct oscillation frequency and wave form [1]. Despite these differences in oscillation properties, SA node cells in the normal heart generate a coherent oscillatory wave known as the pacemaker potential which propagates throughout the heart to stimulate contraction of the atria and ventricles. The process by which cells within the node lock onto a common oscillation frequency is known as frequency entrainment.

Pacemaker synchronization has been studied using simplified models such as networks of pulse-coupled oscillators [2] in which each oscillator has identical frequency but different phase. More recently, synchronization of a pair of pulse-coupled oscillators with different oscillation frequency has been investigated [3]. Perhaps the most notable conclusion of this study was the lack of non-periodic dynamics such as quasiperiodic or chaotic motion as coupling strength was varied. More biophysically detailed models of pacemaker synchronization [4] in conjunction with experimental studies [4,5] have provided strong support for the idea that frequency entrainment is a consequence of ionic current flow through gap junction channels interconnecting neighboring cells. While the density of gap junction channels is high in atrial and ventricular tissue, it is low within the sino-atrial node [6]. This raises the question of how synchronization of pacemaker cells can be achieved with only a low density of gap junction channels coupling each cell.

We have been studying this problem using physiologically detailed models of single rabbit SA node cells, with model parameters adjusted to fit experimental data on regional variation of cell oscillation properties. These studies have shown that as few as 4–5 gap junction channels (each with a coupling conductance of 50 pS) are sufficient to account for frequency entrainment in both cell pairs and large cell networks [7]. Furthermore, it was found that at least four dynamic regimes exist as coupling conductance is increased. These regimes are characterized by (1) independent oscillation, (2) quasiperiodic oscillation, (3) frequency entrainment, and (4) wave form entrainment.

In this Letter, we present evidence of additional regimes of complex dynamics. Results are based on numerical bifurcation analyses of resistively coupled model cell pairs. At low coupling conductance, we demonstrate the existence of period-k limit cycles interspersed between quasiperiodic regimes. At somewhat higher coupling conductance, we demonstrate a period-doubling cascade to chaos [8]. At still higher coupling, we demonstrate bifurcation to a periodic orbit corresponding to frequency entrainment. The relationship of these complex dynamics to the origin of certain cardiac arrhythmias will be discussed.

The SA node cell model used is that of Noble and his colleagues and is based directly on voltage-clamp data obtained from isolated cells. Detailed descriptions of the model are given in [9]. Time- and voltage-dependent properties of membrane currents are modeled using equations of the form proposed originally by Hodgkin and Huxley [10], with parameters adjusted to fit the voltage-clamp data. An expression for the kth voltage-dependent outward membrane current $I_k(V_t)$ is

$$I_k(V_t) = (V_t - E_k) G_k^{\max} m_k(V_t)^{p_k} h_k(V_t)^{q_k}, \quad (1)$$

$$\dot{m}_k(V_t) = \alpha_k^m(V_t)[1 - m_k(V_t)] - \beta_k^m(V_t) m_k(V_t), \quad (2)$$

$$\dot{h}_k(V_t) = \alpha_k^h(V_t)[1 - h_k(V_t)] - \beta_k^h(V_t) h_k(V_t), \quad (3)$$

where V_t is trans-membrane potential, E_k is the reversal potential of the ion(s) to which the kth membrane conductance is permeable, and $G_k^{\max}$ is the peak conductance of the kth voltage-dependent membrane conductance. The peak conductance is multiplied by a factor m_k, raised to the p_kth power. This factor assumes values between 0 and 1, and models activation of the kth membrane current. $G_k^{\max}$ is also scaled by a factor h_k, raised to the q_kth power. This factor ranges from 1 to 0, and models inactivation of the kth membrane current. Activation and inactivation variables m_k and h_k are solutions of the nonlinear ordinary differential equations (2) and (3).

The functions $\alpha_k^{m,h}(V_t)$ and $\beta_k^{m,h}(V_t)$ are forward and backward voltage-dependent rate constants for the activation and inactivation variables m_k and h_k. Whole-cell voltage-clamp experiments provide the data required to estimate $G_k^{\max}$, $a_k^{m,h}(V_t)$, and $B_k^{m,h}(V_t)$. Eight distinct membrane currents are modeled: (a) I_f—a hyperpolarizing activated current carried by sodium (Na) and potassium (K) ions; (b) I_K—a delayed K current; (c) I_{K1}—an instantaneous K current; (d) I_{Na}—a fast inward Na current; (e) $I_{si,Ca}$ and $I_{si,K}$—calcium (Ca) and K components of the second inward current; and (f) $I_{b,Na}$ and $I_{b,Ca}$—linear background Na and Ca currents.

The model also includes descriptions of the Na-K energy-dependent pump current $I_{Na\text{-}K}$ and the Na-Ca exchange current $I_{Na\text{-}Ca}$. Outward current through the kth membrane ion pump exchanger is modeled as an instantaneous function of the intra- and extracellular concentrations ($[C_i^{m,n}]$ and $[C_o^{m,n}]$, respectively) of the relevant ionic species m and n, and of membrane potential V_t:

$$I_k^{pe} = f_k([C_o^{m,n}],[C_i^{m,n}],V_t). \quad (4)$$

Cells are coupled by a conductor G_c, yielding the following expression for the time rate of change of membrane potential in the two cells (denoted by superscripts 1 and 2):

$$\dot{V}_t^1 = \left[-\sum_k I_k^1(V_t^1) - \sum_k I_k^{1,pe} + (V_t^2 - V_t^1)G_c\right] \Big/ C_m^1, \quad (5)$$

$$\dot{V}_t^2 = \left[-\sum_k I_k^2(V_t^2) - \sum_k I_k^{2,pe} + (V_t^1 - V_t^2)G_c\right] \Big/ C_m^2, \quad (6)$$

where C_m^j is membrane capacitance of the jth cell. Intracellular concentrations of Na, Ca, and K vary in time. The time rate of change of the concentration of the kth ionic species is

$$[\dot{C}_k] = \sum_k I_k^{total}/z_k F V_{eff}, \quad (7)$$

where $-I_k^{total}$ is the total inward current associated with the kth ionic species, V_{eff} the effective cell volume, F Faraday's constant, and z_k the valence of the kth ionic species. Sequestration and release of Ca from intracellular organelles is modeled using a set of three first order differential equations. These equations specify the net Ca current I_{up} pumped into organelles (uptake pool), the net Ca current I_{rel} released from intracellular stores (release pool) when the cytosolic level of Ca exceeds a threshold value, and the net Ca current I_{tr} corresponding to transfer of Ca from the uptake to the release pool.

All told, the model yields a system of 14 nonlinear ordinary differential equations describing each cell. The detailed equations and parameter values can be found in [9]. For a pair of coupled SA node cells, the phase-space dimension is 28. Gap junction coupling was modeled using fixed linear conductor; neither stochastic gating of gap junction channels nor voltage-dependent effects were considered [11]. This system was integrated using an adaptive step fourth order Runge-Kutta algorithm. Differences in cell oscillation frequency and wave form of the two cells are modeled by adjusting parameters of membrane currents so as to match data recorded from pacemaker cells in different regions of the SA node [1,7]. For the data in this paper, oscillation periods of the two cells were set to 276 and 347 msec. Figure 1 shows the time-varying membrane potential of the two model cells.

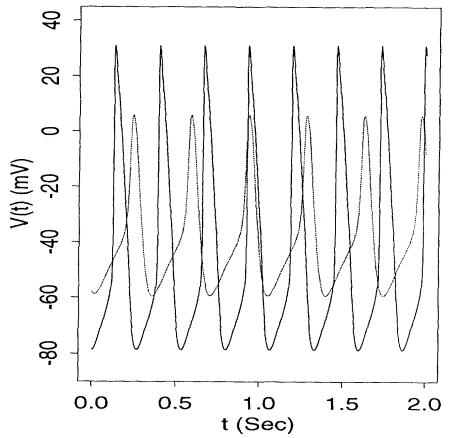

FIG. 1. Membrane potential (ordinate, mV) versus time (abscissa, sec) for two uncoupled model cells, one with oscillation period 347 msec (dotted line), and another with oscillation period 267 msec (solid line).

The asymptotic behavior of the coupled cell equations is governed by low-dimensional attractors [7]. Dynamics can therefore be studied using the delayed-coordinate embedding technique [12]. In this method, a k-dimensional embedding space is constructed using time lagged values of the membrane potential computed for one cell, $\{V(t),V(t-\tau),V(t-2\tau),\ldots,V(t-(k-1)\tau)\}$, by integrating the system of 28 differential equations defining the two coupled cells for 100 sec to establish a set of initial conditions. An additional 100 sec integration is then performed, saving output values every 50 μsec. The resulting time series is used to reconstruct attractors. For most of the parameter regimes studied, the final attractors are periodic orbits and two-dimensional tori and, hence, $k=3$ is sufficient to describe the dynamics in such cases. However, we have also used $k=3$ to detect possible chaos. To better visualize the structure of the attractor, we use the Poincaré surface of section to reduce the attractor to a plane. A surface of section consisting of a set of discrete points represents a limit cycle, and closed curves represent quasiperiodic orbits. Open, more complicated curves may indicate chaotic motion.

Figure 2 shows examples of attractors and surface of sections for representative values of coupling conductance G_c. In Fig. 2(a), the attractor was computed at a coupling conductance of $G_c=70$ pS, and is clearly toroidal in shape. Figure 2(b) shows the surface of section. For cases studied in this paper, the surface of section is generated by cutting the flow with a plane positioned at $V(t)=-10$ mV. Two closed curves on the surface of section demonstrate that the flow is two-frequency quasiperiodic. Figure 2(c) shows the attractor at the coupling

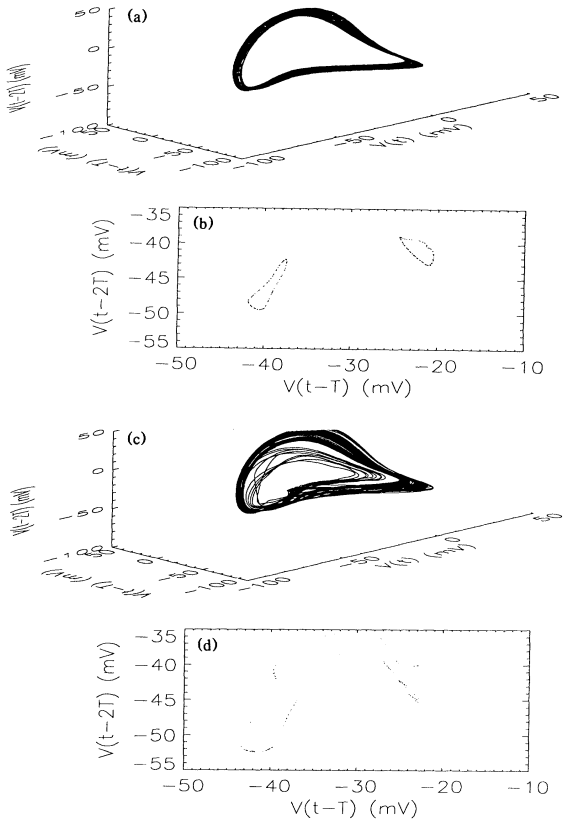

FIG. 2. (a) Three-dimensional reconstruction (using the delay-coordinate embedding technique) of a torus; coupling conductance $G_c = 70$ pS. (b) Poincaré surface of section of (a) at $V(t) = -10$ mV. (c) Three-dimensional reconstruction attractor reconstruction at a coupling conductance $G_c = 152$ pS. (d) Surface of section of (c) at $V(t) = -10$ mV.

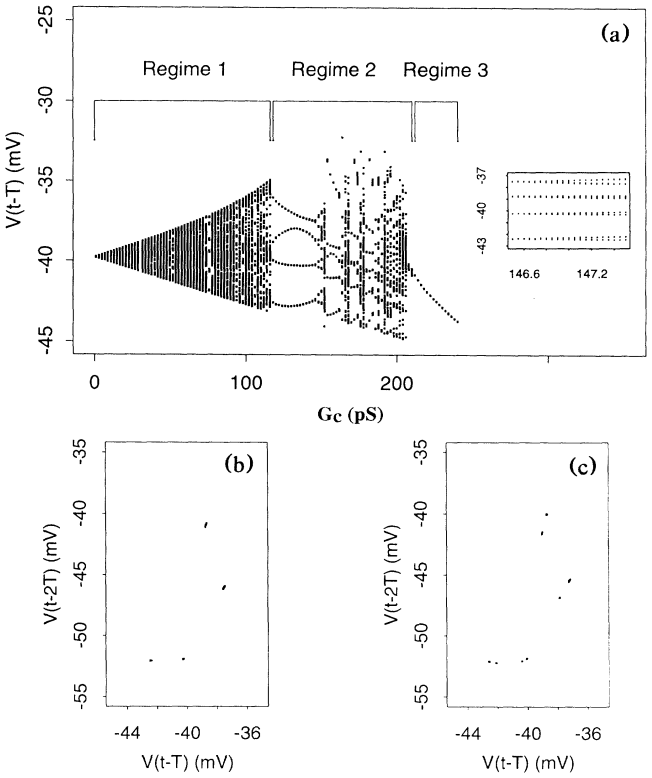

FIG. 3. (a) Bifurcation diagram illustrating three dynamic regimes: $G_c < 116$ pS (regime 1), $116 \leq G_c < 212$ pS (regime 2), and $G_c \geq 212$ pS (regime 3). Diagram was computed by projection of one-sided surface of sections computed at various coupling values (abscissa, pS) onto the $V(t-\tau)$ axis (ordinate, mV). A high resolution plot around $G_c = 147$ pS is shown in the inset of (a). (b) Surface of section showing a period-4 trajectory at coupling conductance 146 pS. (c) Surface of section showing a period-8 trajectory at the coupling conductance 148 pS.

conductance $G_c = 152$ pS, and Fig. 2(d) shows the surface of section. The complex arrangement of scattered points in Fig. 2(d) indicates the trajectory in Fig. 2(c) may be chaotic.

Figure 3(a) is a bifurcation diagram summarizing the results of computing Poincaré surface sections for coupling values in the range of 1 to 240 pS in steps of 2 pS. At each coupling conductance (abscissa), one-sided sections were projected onto the $V(t-\tau)$ axis (ordinate). With this approach, motions on a period-k limit cycle project to k discrete points. For quasiperiodic motion, projections will ideally form one line segment (if there are a sufficient number of points on the section). Projections for chaotic motion will form a number of short line segments after projection. Hence, in practice projections of sections for quasiperiodic and chaotic motions are difficult to distinguish. In such cases we have therefore examined the trajectories on the surface of section to distinguish between these two types of motion.

Figure 3(a) demonstrates three major dynamic regimes corresponding to $G_c < 116$ pS (regime 1), $116 \leq G_c < 212$ pS (regime 2), and $G_c \geq 212$ pS (regime 3). For most G_c values in regime 1, the motion is quasiperiodic. However, there also exist conductance values for which the attractor is periodic. For instance, a period-6 attractor occurs at $G_c = 76$ pS. The occasional coupling values giving rise to periodic attractors are interspersed between those producing quasiperiodic attractors. This is known as the Arnold's tongue phenomena, and has been studied extensively for the family of circle maps [13].

At $G_c \approx 116$ pS, the quasiperiodic attractor collapses into a period-4 attractor [as shown in Fig. 3(b)]. As G_c is increased, the system goes through a period-doubling cascade and becomes chaotic at $G_c \approx 152$ pS. This period-doubling cascade is confirmed by computing the surface of sections at different conductance values to identify successive period-8 [as shown in Fig. 3(c)], and period-16 (not shown, but computed) attractors, and so on. To see the first period-doubling bifurcation clearly, a high resolution plot around $G_c = 147$ pS is shown in the

inset of Fig. 3(a). Note that determination of Fig. 3(a) is computationally demanding. Hence, it is not realistic to make a high resolution plot of the bifurcation diagram for the entire parameter range considered. The final attractor at $G_c = 152$ pS has a positive largest Lyapunov exponent, which we estimate to be approximately 0.16 by tracking the exponential separation rate of an ensemble of nearby initial condition pairs. The positivity of the largest Lyapunov exponent indicates that the attractor at this conductance value is chaotic (see below for physiological significance of an appearance of the chaotic attractor). To test whether the chaotic behavior is transient, we have used longer initial integration time up to 800 sec. It is found that the chaotic behavior remains the same. As G_c increases further, period-5, -6, and -7 windows are observed. These behaviors have been observed in other chaotic dynamical systems [14]. Finally, for $G_c \geq 212$ pS (regime 3), the attractor becomes a period-1, signifying frequency entrainment of the two cells [7].

Recent measurements of coupling conductance between pairs of SA node cells indicate that a typical cell-to-cell coupling value is 2.5 nS, or about 50 channels [5]. Our results demonstrate that this level of coupling is about 10 times greater than that required for frequency entrainment. Thus, coupling in the normal SA node is sufficiently large to assure an order of magnitude "safety margin" for frequency entrainment. However, gap junction channel conductance is modulated by factors such as pH, and internal calcium concentration [15]. In particular, Noma and Tsuboi [15] have demonstrated an order of magnitude reduction of gap junction conductance between cardiac myocytes upon increasing cytosolic Ca levels from about 40 to 400 nM. Therefore, factors which act to increase intracellular Ca levels could produce substantial reduction of gap junction conductance. It is well established that one consequence of ischemia in cardiac tissue is an increase in intracellular Ca levels that occurs over a time course of tens of minutes [16]. We therefore hypothesize that arrhythmias induced by ischemia may in part result from a gradual drift of coupling through the regimes of quasiperiodic and chaotic dynamics shown in Fig. 3.

This work was supported by NSF Grant No. DIR 91-17874 (R.L.W.), the Whitaker Foundation, and U.S. Army Research Office Contract No. DAAL03-89-C-0038 to the Army High Performance Computing Research Center at the University of Minnesota.

[1] I. Kodama and M. Boyett, Pflugers Arch. **404**, 214 (1985); H. Honjo and M. R. Boyett, J. Physiol. (London) **452**, 128 (1992).

[2] A. T. Winfree, *The Geometry of Biological Time* (Springer-Verlag, New York, 1980); C. S. Peskin, *Mathematical Aspect of Heart Physiology* (Courant Institute of Mathematical Science, New York University, New York, 1975); R. E. Mirollo and S. H. Strogatz, SIAM J. Appl. Math. **50**, 1645 (1990).

[3] A. A. Brailove, Int. J. Bifurcation Chaos **2**, 341 (1992).

[4] J. Jalife, J. Physiol. (London) **356**, 221 (1984).

[5] J. M. B. Anumonwo, H. Z. Wang, E. Trabka-Janik, B. Dunham, R. D. Veenstra, M. Delmar, and J. Jalife, Circ. Res. **71**, 229 (1992).

[6] M. Masson-Pevet, W. K. Bleeker, A. J. C. Mackaay, and L. N. Bouman, J. Molec. Cell. Cardiol. **11**, 555 (1979); W. K. Bleeker, A. J. C. Mackaay, M. Masson-Pevet, L. N. Bouman, and A. E. Becker, Circ. Res. **46**, 11 (1980).

[7] D. Cai, R. Winslow, and D. Noble, in *Computer in Cardiology Proceedings 1992* (IEEE Computer Society Press, New York, 1992), p. 579; R. L. Winslow, A. Varghese, D. Noble, J. C. Denyer, and A. Kimball, J. Physiol. (London) **446**, 242 (1992); R. L. Winslow, A. Kimball, A. Varghese, and D. Noble, Physica (Amsterdam) **64D**, 281–298 (1993).

[8] M. J. Feigenbaum, J. Stat. Phys. **19**, 25 (1978).

[9] D. Noble and S. Noble, Proc. R. Soc. London B **222**, 295 (1984); H. F. Brown, J. Kimura, D. Noble, and S. Noble, Proc. R. Soc. London B **222**, 329 (1984); D. Noble, D. DiFrancesco, and J. Denyer, in *Neuronal and Cellular Oscillators*, edited by J. W. Jacklet (Marcel Dekker, New York, 1989); D. Noble, *OXSOFT Heart Program Manual* (OXSOFT Ltd., Oxford, England, 1990); D. Noble, J. C. Denyer, H. F. Brown, and D. DiFrancesco, Proc. R. Soc. London B **250**, 199 (1992); D. Noble, J. Denyer, H. F. Brown, R. L. Winslow, and A. Kimball, in *Coupled Oscillators*, edited by J. G. Taylor and C. L. T. Mannion (Springer-Verlag, Berlin, 1992).

[10] A. L. Hodgkin and A. F. Huxley, J. Physiol. (London) **117**, 500 (1952).

[11] Effects of stochastic gating of gap junction channels on frequency entrainment have been studied by R. Wilders (Ph.D. dissertation, University of Amsterdam, 1993). Because of the long mean open time of these channels, such effects are of second order importance. Gap junction coupling may be voltage dependent. Voltage dependence has been determined in coupled atrial cells [R. Lal and M. F. Arnsdorf, Circ. Res. **71**, 737 (1992)]. On the other hand, ventricular cell coupling appears to be independent of transjunctional voltage [15]. Sino-atrial cell gap junctions exhibit weak voltage dependence, and are linear over much of the transjunctional voltage range [5].

[12] F. Takens, in *Dynamical Systems and Turbulence*, edited by D. Rand and L.-S. Young (Springer-Verlag, Berlin, 1981).

[13] L. Glass and M. C. Mackay, *From Clocks to Chaos, The Rhythms of Life* (Princeton Univ. Press, Princeton, 1988).

[14] E. Ott, *Chaos in Dynamical Systems* (Oxford Univ. Press, New York, 1992).

[15] A. Noma and N. Tsuboi, J. Physiol. (London) **382**, 193 (1987).

[16] C. Steenbergen, E. Murphy, J. A. Watts, and R. London, Circ. Res. **66**, 135 (1990); **60**, 700 (1987); Y. Koretsune and E. Marban, Am. J. Physiol. **258**, H9 (1990); E. Marban, M. Kitakaze, H. Kusuoka, J. K. Porterfield, D. T. Yue, and V. P. Chacko, Proc. Natl. Acad. Sci. U.S.A. **84**, 6005–6009 (1987).